Nanoscale

Large Two-Photon Cross Sections and Low-Threshold Multiphoton Lasing of CdS/CdSe/CdS Quantum Shells

Journal:	*Nanoscale*
Manuscript ID	NR-ART-08-2023-004203.R1
Article Type:	Paper
Date Submitted by the Author:	30-Sep-2023
Complete List of Authors:	Diroll, Benjamin; Argonne National Laboratory, Center for Nanoscale Materials Cassidy, James; Bowling Green State University Harankahage, Dulanjan; Bowling Green State University, Department of Physics and Astronomy Hua, Muchuan; Argonne National Laboratory, Nanoscience and Technology Lin, Xiao-Min; Argonne National Laboratory, Materials Science Division; Bldg. 200 Zamkov, Mikhail; Bowling Green State University,

ARTICLE

Large Two-Photon Cross Sections and Low-Threshold Multiphoton Lasing of CdS/CdSe/CdS Quantum Shells

Received 00th January 20xx,
Accepted 00th January 20xx

DOI: 10.1039/x0xx00000x

Benjamin T. Diroll,[a*] James P. Cassidy,[b] Dulanjan Harankahage,[b] Muchuan Hua,[a] Xiao-Min Lin,[a] Mikhail Zamkov[b]

Colloidal quantum shells are spherical semiconductor quantum wells, which have shown strong promise as optical materials, particularly in classes of experiments requiring multiple excitons. The two-photon properties of CdS/CdSe/CdS quantum shell samples are studied here to demonstrate large non-linear absorption cross-sections while retaining advantageous multiexciton physics conferred by the geometrical structure. The quantum shells have large two-phonon cross sections (0.4-7.9×10^6 GM), which highlights their potential use in upconversion imaging in which large per particle two-photon absorption is critical. Time-resolved measurements confirmed that the quantum shells have long biexciton lifetime (>10 ns in the largest core samples reported here) and large gain bandwidth (>300 meV). The combination of these attributes with large two-photon cross sections makes the CdS/CdSe/CdS quantum shells excellent gain media for two-photon excitation. With a broad gain bandwidth and long gain lifetime, quantum shell solids support multimodal amplified spontaneous emission from excitons, biexcitons, and higher excited states. Thresholds for amplified spontaneous emission and lasing, which are as low as 1 mJ·cm^{-2}, are comparable to, or lower than, the thresholds reported for other colloidal materials.

Introduction

Colloidal quantum shells (QSs), in which a narrow band gap spherical shell is sandwiched between a wider band gap core and a surface layer, have recently shown promise as nanoscopic optical materials.[1–9] They offer a distinct form of quantum confinement based upon the thickness of the shell material, between that of flat quantum wells and quasi-spherical quantum dots.[1,3,10–17] Although there are a number of QS structures, the most sophisticated in terms of synthetic development are concentric CdS/CdSe/CdS nanostructures, in which quantum confinement of the CdSe layer dictates their optical properties.[1,15] The large physical dimensions of QSs, which have been prepared with diameters greater than 15 nm,[1] decouples the physical size of the nano-object from quantum confinement.[10,15] Interactions between carriers are further suppressed by the type II alignment of the bands.[18,19] An important result of this dimensionality control is the highly-effective suppression of Auger recombination, resulting in long biexciton lifetimes, more radiative emission from biexcitonic states, long optical gain lifetime, and broad optical gain bandwidths.[2,7–9,20]

This work leverages these promising elements of QS materials with below band gap excitation to demonstrate their utility in two-photon applications. Non-linear optical properties and two-photon absorption in particular is important for imaging and microscopy resolution, particularly in biology,[21,22] and valuable for optically-pumped laser applications in which frequency upconversion is desired.[23–35] Here, it is found that the CdS/CdSe/CdS QSs have large two-photon cross sections of 0.4-7.9 10^6 GM, indicating that such QS are potentially useful agents for imaging and tagging. A combination of advantageous multiexciton properties and large two-photon cross sections of QSs has been utilized to showcase low-threshold multiphoton excited optical gain, amplified spontaneous emission, and lasing. Optical pumping thresholds as low as1 mJ·cm^{-2} have been achieved.

Results and Discussion

Figure 1 shows structural and optical characterization of the QS samples used in this work, which are identified by their respective CdS core sizes. The core/shell/shell geometry of the samples was obtained by the triple-stage colloidal growth procedure, similar to earlier works.[2,20] The concentric core/shell/shell geometry is apparent in dark field images in Figures 1a-1cwith the inset of Figure 1a showing the idealized cross-section. Enhanced contrast of the core/shell interface may derive both from composition (Z-contrast) and strain at the interface.[36] The dark field image in Figure 1c is also accompanied by an elemental map of the QS showing that sulfur is enriched in the core and outer ring whereas selenium is enriched along an intermediate ring, as expected form the cross-sectional view of the idealized geometry. Additional microscopy images can be found in Figure S2 and sizing data is reported in Table 1. Absorption and photoluminescence spectra are shown in Figure 1d. Due to the large volume of CdS, the absorption above 2.5 eV is much larger than the absorption of the CdSe QS, but photoluminescence under all excitation regimes used in this work derives only from narrower band gap CdSe. Quantum yields of the samples (reported in Table 1) with comparatively large cores used in this work, which exceed the Bohr exciton size of CdS, are lower than previous reports,[37] most likely due to poorer surface passivation of the large emitter interfaces. As

[a] Center for Nanoscale Materials, Argonne National Laboratory. 9700 S. Cass Avenue, Lemont, Illinois 60439, United States Address here.
[b] The Center for Photochemical Sciences and Department of Physics, Bowling Green State University, Bowling Green, Ohio 43403, United States.
*bdiroll@anl.gov

Electronic Supplementary Information (ESI) available: additional experimental details and data may be found in the ESI. See DOI: 10.1039/x0xx00000x

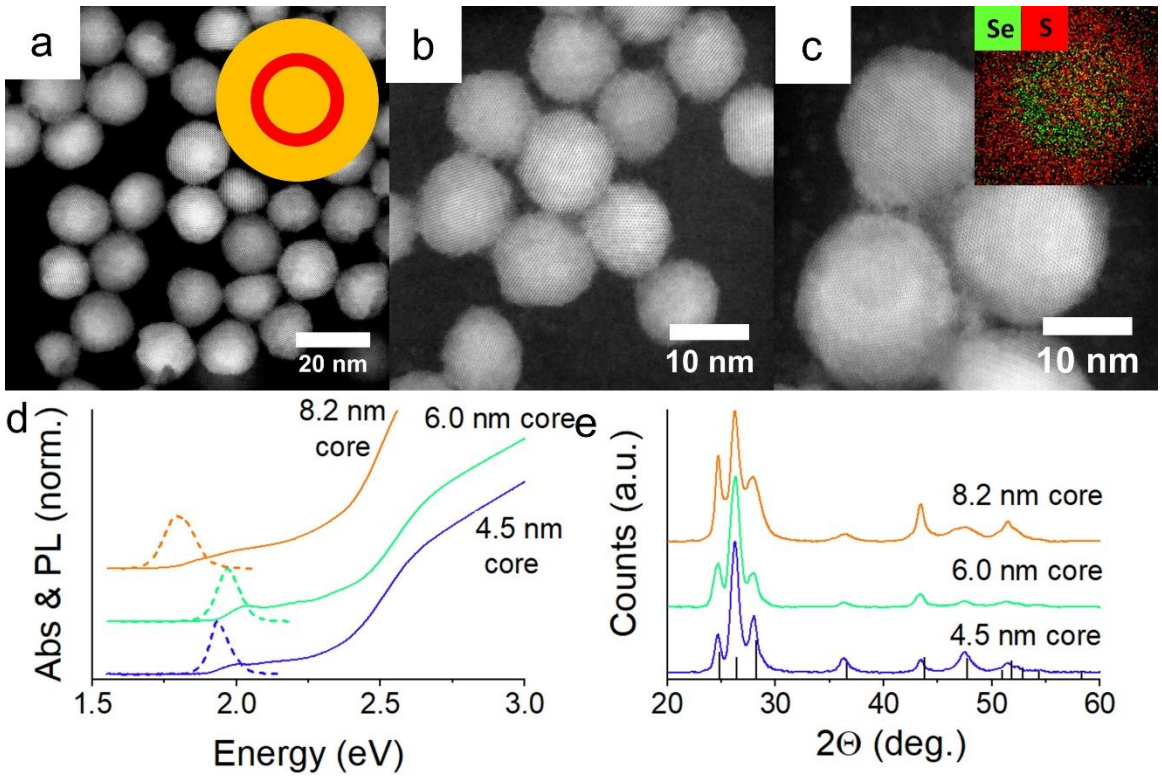

Figure 1. (a-c) Dark field transmission electron microscopy images of (a) 4.5 nm core QSs, (b) 6.0 nm core QSs, and (c) 8.2nm core QSs. Inset in (a) is a cartoon of the QS structure comprised of an inner CdS core and concentric shells of CdSe and CdS. Inset in (c) is an elemental map made using energy-dispersive X-ray analysis of sulfur (red) and selenium (green) showing the concentric ring structure. (d) Absorption (solid lines) and photoluminescence (dashed lines) of CdS/CdSe/CdS QS samples. (e) Powder X-ray diffraction of the QSs. Black vertical lines indicate the reflections of wurtzite CdS, JCPDS card no. 77-2306.

shown in Figure 1e QSs have a wurtzite crystal structure slightly larger in lattice constant than CdS, the dominant constituent of the QSs.

Representative fluorescence data from the QS samples under two photon excitation is shown in Figure 2a using the sample with 4.5 nm CdS cores. Figure 2a shows the intensity-dependent spectra for the 4.5 nm CdS core sample and Figure 2b shows a log-log plot of the power-dependent emission for all three samples which confirms the two-photon absorption process with slopes of 1.99±0.02, 2.08±0.02, and 2.01±0.01 for 4.5 nm, 6.0 nm, and 8.2 nm QS cores, respectively. Figure 2c show the spectra normalized at the peak intensity. At low intensity, the spectra of the samples under one- and two-photon excitation are superimposable (Figure 2d). At higher intensities, such as the higher power two-photon excitation shown in Figure 2c, there is an increase in intensity of the blue side of the photoluminescence feature. This feature, which is common to the QSs, is due to emission from doubly-excited biexciton emission. In particular, the blueshift observed with respect to the exciton emission is, for these CdS/CdSe/CdS QDs, is due to a repulsive biexciton binding energy—slightly higher in energy than excitons. For the QS samples, this biexciton binding energy ($E_{b,xx}$) is estimated by comparing the ASE peak (see below) to the low-fluence PL peak as -49 meV, -53 meV, and -48 meV for the 4.5 nm, 6.0 nm, and 8.2 nm cores, respectively. The repulsive biexciton energies confirm a type-II or quasi-type II band alignment, with substantial delocalization of the electron into CdS, similar to what is observed in certain CdSe/CdS NRs.[38,39] The repulsive biexciton energies are substantially larger than those found in "giant" quantum dot systems.[40] Formation of

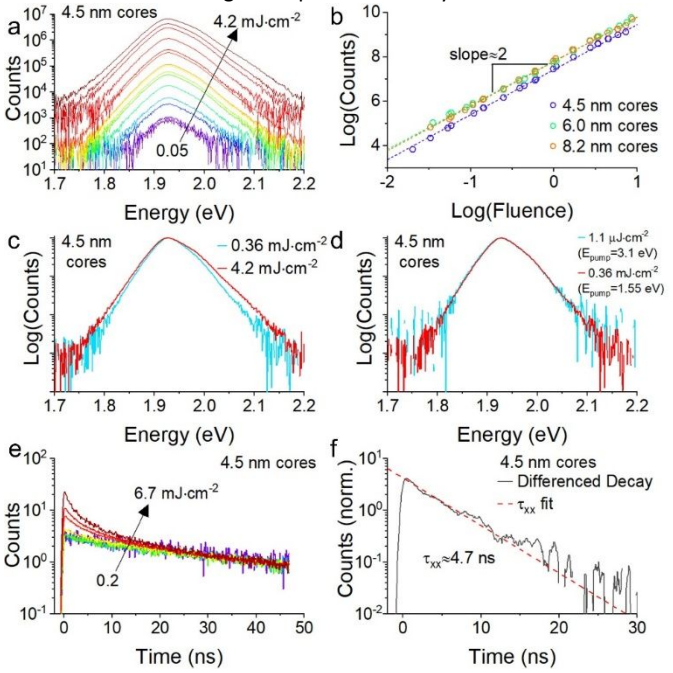

Figure 2. (a) Photoluminescence intensity with increasing pump 1.55 eV (800 nm) pump fluence for sample 4.5 nm core QSs. (b) Log-Log plot of integrated photoluminescence counts versus fluence for the three QS samples. Log of fluence is taken for the value in mJ·cm^{-2}. (c) Normalized spectra of 4.5 nm core QSs at different specified pump

fluences. Dashed lines indicate linear slopes of close to 2 for each. (d) Normalized photoluminescence spectrum of 4.5 nm core QSs with specified fluences of 3.10 eV and 1.55 eV excitation. (e) Time-resolved photoluminescence of 4.5 nm core QSs normalized at ~50 ns delay for a series of increasing pump fluence. (f) Differenced data from (e) showing the residual counts from data collected at a fluence of 1.58 mJ·cm^{-2} after subtracting the average counts of 0.24-0.61 mJ·cm^{-2}. A dashed red line indicates a monoexponential fit to estimate the biexciton lifetime under two photon excitation.

Table 1. Sizing and extinction properties of quantum shell samples

Core[a] (nm)		V_{total}[a] (nm^3)	E_{PL} (eV)	ε[b] (×10^{-7} M^{-1}cm^{-1})	σ$^{(1)}$[b] (×10^{-13} cm^2)	σ$^{(2)}$[c] (×10^6 GM)	
4.5±0.3		678±162	1.925	3.2±0.9	1.2±0.3	1.7±0.5	
6.0±0.5		1630±466	1.954	1.3±0.3	0.5±.1	0.4±.1	
8.2±0.8		3764±1100	1.774	7.6±2.2	2.9±0.8	7.9±2.3	

[a] Estimated from TEM sizing. Core, V_{total} the core diameter, and total volume of the structure, respectively. Errors are standard deviation.
[b]Molar extinction coefficient (ε) and one-photon cross section (σ$^{(1)}$) at 3.1 eV, based upon ICP of solutions with known absorption, using TEM-based sizing.
[c]Two-photon cross-section at 1.55 eV (800 nm), calculated from photoluminescence intensity versus Rhodamine 6G standard with two-photon excitation according to literature methods.

biexcitonic species is also manifest through the emergence of a faster decay feature in fluence-dependent time-resolved photoluminescence data in Figure 2e. Following Klimov,[41] differencing normalized dynamics above the threshold at which biexcitonic decay is apparent and low-fluence data with two-photon excitation yields an estimate of the biexciton lifetime, here of 4.7 ns. This is smaller than to the biexciton lifetime extracted under more reliable one-photon excitation (see Supporting Information Figures S2 and S3). The biexciton lifetime of the 6.0 nm core and 8.2 nm core samples are 6.7 ns and 11.9 ns, respectively (see Table 2). Biexciton lifetimes in nanosecond time-range are a consequence of the repulsive nature of exciton-exciton interactions and the geometry of the QSs, which suppresses Auger recombination rates, the primary mechanism of biexciton recombination in semiconductor nanocrystals.[41] Biexciton lifetimes are important for determining the threshold of lasing under continuous or electrical injection and these QS show among the longest biexciton lifetimes of nanocrystal systems.[42] The 8.2 nm QSs in particular exhibit the longest reported biexciton lifetime reported using this measurement technique. The biexciton lifetimes of the QS samples are, for example, far exceed the hundreds of picoseconds of CdSe dots,[43] core/shell structures with sharp interfaces,[44,45] and nanoplatelets[46]; the ensembles of QSs show longer biexciton lifetimes than even the best single particle measurements of graded core/shells with suppressed Auger.[44,47,48]

The two-photon cross sections of the samples was calculated using an approach developed earlier,[49,50] in which standards of known quantum yield and two photon cross section are used similar to the calculation of comparative quantum yield. According to this methodology, the two-photon cross section of an unknown ($\sigma_x^{(2)}$) depends on the one-photon cross section ($\sigma_x^{(1)}$), fluorescence intensity under one- and two-photon excitation ($F_x^{(n)}$), and quantum yields (η) of the unknown and a reference dye:

$$\sigma_x^{(2)} = \frac{\sigma_{ref}^{(2)}\sigma_x^{(1)}}{\sigma_{ref}^{(1)}} \cdot \frac{F_x^{(2)}}{F_{ref}^{(2)}} \cdot \frac{F_{ref}^{(1)}}{F_x^{(1)}}$$

This equation is only true if the quantum yield of the sample and the reference dye are assumed to be the same under both one-and two-photon excitation ($\eta^{(2)} = \eta^{(1)}$), an assumption which is substantiated here by identical lifetime (Figure S5) and spectrum of the fluorescence (Figure 2d) under one- and two-excitation.[49] Several parameters can be measured directly or inferred; parameters of the reference dye, Rhodamine 6G (which has weak but quantified $\sigma^{(1)}$ and $\sigma^{(2)}$ at relevant energies), are taken from literature.[51–53] The cross-section of the samples is ascertained through measurement of the cadmium concentration of digested QSs with measured absorption and particle size estimated from TEM (Table 1), using inductively-coupled plasma optical emission spectroscopy (ICP-OES). Extinction coefficients and one-photon cross-sections calculated using this method for the samples used in this work are given in Table 1. The ratio of $F_x^{(1)}/F_{ref}^{(1)}$ is the ratio of quantum yields under one-photon excitation; the ratio $F_{ref}^{(2)}/F_x^{(2)}$ is calculated from fluence-dependent two-photon photoluminescence. The two-photon cross-sections of the QS samples at 1.55 eV (800 nm), in Goeppert-Mayer (GM) units, ranged from 0.4-7.9×10^6 GM. On an absolute scale, such two-photon cross sections are comparable to the very large cross sections reported for cadmium selenide nanoplatelets at the same energy,[49] which substantially exceed those of QDs or CdSe/CdS nanorods, for which reach 10^4 GM and 10^5 GM, respectively.[49,54] Large per particle two-photon cross sections marks the QSs out as strong candidates for two-photon imaging applications, such as biolabeling, where the absolute amount of light emission from individual particles is critical. QSs also achieve these high cross sections without the large degree of sensitivity to surface modification and mechanical deformation and in nanoplatelets.[55,56] On a volumetric basis ($\sigma_x^{(2)}/V$), the QSs have two-photon cross sections which range from 0.6-2.1×10^{-26} cm·s, which falls above values of quantum dots but below most nanoplatelets.[49] This suggests that the advantages of the two-dimensional nanoplatelet geometry for two-photon absorption can be partially recaptured in QSs, although most two-photon absorption is still occurring in the CdS layers.

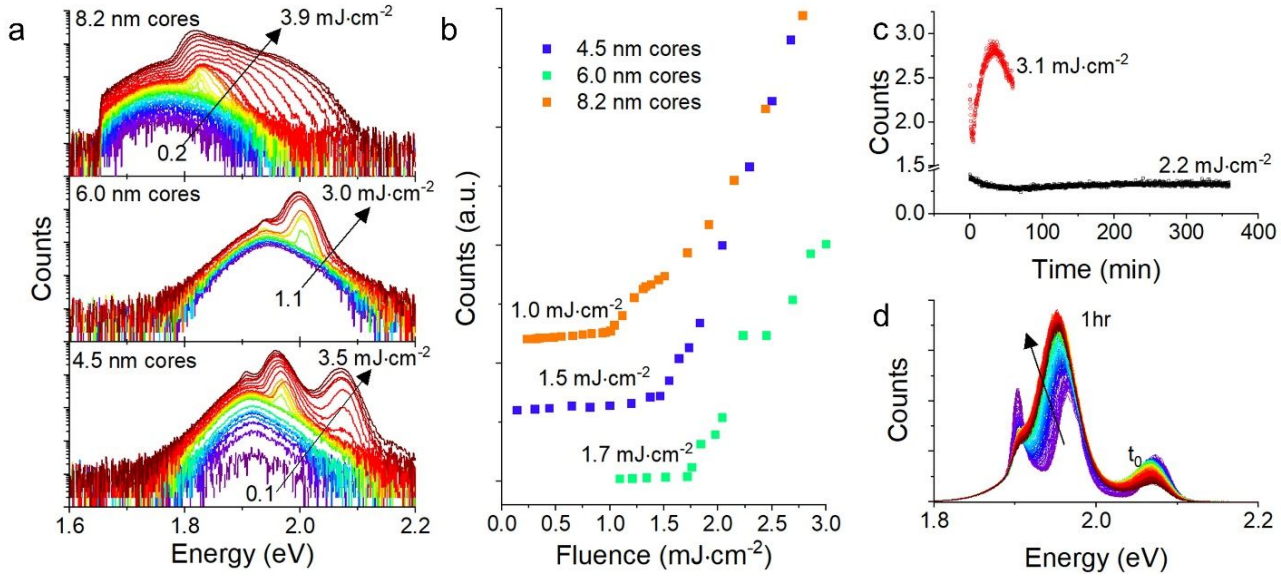

Figure 3. (a) Emission spectra as a function of fluence for CdS/CdSe/CdS QS thin film samples as a function of excitation fluence at 1.55 eV. A 750 nm short pass filter is used to block the pump light. (b) Emission counts of QS thin film samples versus laser fluence. (c) Integrated counts of 4.5 nm core QSs two values of fluence above the amplified spontaneous emission threshold. Data represents total integrated counts versus time. (d) Spectra of sample 4.5 nm core QSs displaying multimodal amplified spontaneous emission held at 3.1 mJ·cm^{-2} by stripe illumination for 1 hour. Violet spectra represent early time and red later times. Spectra were collected every 15 seconds for 1 hour.

Given the large two-photon cross sections and previous demonstrations of low-threshold optical amplification, two-photon excitation was used to measure amplified spontaneous emission and lasing from the QS samples. Compared to one-photon excitation, frequency upconverting optical gain has advantages in homogeneity of excitation through the medium, weaker scattering of the pump excitation, and ease of cavity design. More generally, upconverted lasing is a useful alternative to non-linear optical conversions of coherent light.[23] To measure optical amplification, thin films of QSs were cast on to glass slides and amplified spontaneous emission (ASE) thresholds were measured by pumping the sample along a narrow stripe using a cylindrical lens. As shown in Figure 3a, each QS sample exhibited ASE, characterized by the thresholded, non-linear emergence of a new, spectrally narrower emission feature. The first ASE feature of the QSs to appear with increasing pump fluence occurs on the blue side of the photoluminescence spectrum, indicating that it arises from a repulsive biexictonic emission.[2,18–20] But, as shown in previous measurements on QS samples,[20] multiple ASE peaks are observed over a wide range of energy. In the cases of the 4.5 nm and 6.0 nm cores, ASE also occurs at an energy near the center of the photoluminescence feature, likely attributable to excitonic emission. For the 4.5 nm core and 8.2 nm cores, higher fluences result in ASE features greater in energy than the biexcitonic emission feature, due to filling of the band edge states. Corresponding transient absorption measurements of the samples (Figure S6) with 1.55 eV pumping confirm that the QSs can support a broad optical gain bandwidth as high as 300 meV and a gain lifetime of 3-6 nanoseconds (see also Table 2), which is consistent with the long biexciton lifetimes. In addition to the spectral changes, ASE thresholds are analyzed in Figure 3b by measuring the emitted photon counts versus fluence, with thresholds apparent from the sharp increase of intensity at fluences ranging from 1.0-1.7 mJ·cm^{-2}. The broad gain bandwidth, long gain lifetimes, and low two-photon ASE thresholds of these QS samples indicate potential for use as broadband gain media in a variety of cavity structures. It should be noted that the average number of electron-hole pairs associated with these observed thresholds, sometimes denoted $\langle n \rangle_{\text{threshold}}$, excitation appears higher under two-photon excitation than under one-photon excitation. The large size of the QSs also raises the possibility, similar to nanoplatelets, that typical exciton counting practices which were developed for quantum dots are not useful descriptions of threshold and can be replaced with threshold *densities*.[57,58] Nonetheless, the comparison is relevant: for example, the 4.5 nm cores show a threshold of ~4.5 excitons per particle[20] when excited with 3.1 eV but is ~7 under 1.55 eV excitation. These numbers are ~3 for 6.0 nm cores and ~16 for 8.2 nm cores. The reason for the increased number threshold under two-photon excitation is unclear, but could be related to differences in the homogeneity of the excitation.[59] Neither is the divergence unique to QSs: although the best nanoplatelet samples show two-photon thresholds near the one-photon threshold, others show higher thresholds.[31]

Additionally, the stability of ASE in the samples was tested in air at room temperature. At modest fluences just above the ASE threshold for 4.5 nm core QSs, amplified emission lost 25 % of intensity over 50 minutes, but recovered over 6 hours (4.3×10^7 laser shots) to 90 % percent of initial signal (Figure 3c). At higher fluence (3.1 mJ·cm^{-2}), multimodal ASE was variable in both intensity and spectral response, also initially falling 25 %, then recovering to greater intensity than observed initially, which was accompanied by a redshift of the ASE bands and an increase in the biexcitonic band at the expense of excitonic and higher multiexciton bands (Figure 3d). Such variability of ASE is only possible due to the wide gain bandwidth of the QSs, but it may occur due to heating of the samples, which redshifts optical transitions,[15,58] or photocharging, which fills excitonic states.[60] In this case, both effects may be occurring, as the biexcitonic ASE feature increases in intensity over time (relative to the excitonic peak), and redshifts. Fundamentally, the persistence of ASE for long periods of time shows that the samples do not undergo runaway heating which leads to quenching of gain (present in nanoplatelets)[58] or even the destruction of the sample. This stability has two hypothesized origins: first the smaller fraction of ligands and

interfaces in the solids and second, the suppression of Auger recombination results in higher quantum efficiencies of *radiative* relaxation from highly-excited states and therefore less heating of the samples.

Table 2. Optical Gain Characteristics of Quantum Shells

Core (nm)	τ_{XX}[a] (ns)	$E_{b,xx}$ (meV)[b]	ASE_{TPA} ($mJ \cdot cm^{-2}$)	G_{time} (ns) [$mJ \cdot cm^{-2}$][c]	$G_{bandwidth}$ (meV) [$mJ \cdot cm^{-2}$, 10 ps delay][c]
4.5	6.7	-49±5	1.5	5.88 (1.54)	277 [1.54]
6.0	4.0	-53±6	1.7	3.43 [3.12]	193 [3.12]
8.2	11.9	-48±7	1.0	4.9 [3.12]	314 [2.19]

[a]Determined from fluence-dependent time-resolved PL with one-photon excitation. Errors are fit errors.
[b]Determined from measurements of ASE center position, compared to the low-fluence photoluminescence emission center. Errors are from the second derivative minimum smoothing.
[c]Brackets inidate the measurement condition; gain time and bandwidth are calculated from the gain spectra and dynamics in Figure S7.

Finally, the QSs were used in an optically-pumped laser cavity. Two-photon pumped laser cavities have been demonstrated with several different nanomaterials, including CdSe quantum dots and platelets,[24,28,29,31,61–63] and perovskites.[64–67] The 8.2 nm core QS sample was deposited as a thin film via drop-casting in the simple laser cavity shown in Figure 4a. Two color-selective mirrors, with high normal-incidence reflectivity at 1.8 eV were sandwiched to form vertical-cavity surface-emitting laser. One mirror was coated with QSs and the other with a thin layer of PMMA to provide a spacer from the first mirror, a strategy employed earlier in similar Bragg grating lasers.[62] Because the mirror is semitransparent to the two-photon pump at 45°, the pump beam excites the sample at this angle, but the emission is monitored from the cavity at normal incidence. As shown in Figure 4b, a narrow emission line emerges at sufficiently high pump fluence. Initially a single laser line was observed at 1.80 eV with a band width of 770 μeV (0.3 nm), but at higher fluence multiple modes are supported. The exact modes observed depend on the measured sample spot in the cavity; multimodal lasing was also previously observed under one-photon excitation in QSs.[68] The intensity of the optically-pumped laser shows clear thresholding behavior plotted in Figure 4c, with a fluence threshold of this laser slightly above 1.1 $mJ \cdot cm^{-2}$. This threshold is slightly above the threshold for ASE of the same sample, but it should also be noted that the input fluence, measured before the sample, is partially diminished by the front mirror of the cavity and therefore the two thresholds are quite similar. A two-photon optically-pumped laser threshold of ~1 $mJ \cdot cm^{-2}$ is far below reported thresholds in quantum dots and (~6 $mJ \cdot cm^{-2}$),[24,61] comparable to the lowest reported threshold for two-photon pumping in pure CdSe nanoplatelets (1.2 $mJ \cdot cm^{-2}$)[31] or dot-in-rod heterostructures (0.99 $mJ \cdot cm^{-2}$),[28] but somewhat above the two-photon laser threshold for engineered CdSe core/shells (0.764 $mJ \cdot cm^{-2}$)[29] or perovskite nanocrystals (0.3 $mJ \cdot cm^{-2}$).[66]

As with ASE measurements above, the stability of the laser cavity emission was measured over time. In this case, initially a single mode is observed, but after 2 minutes, two laser modes are observed for the sample, both of which shift to the blue over time. In this case, the shift is approximately 10 meV in 30 minutes of measurement. Similar shifts in the mode of whispering gallery mode lasers from semiconductor nanocrystals were recently reported and attributed to changes in the index of the nanocrystal layer due to photocharging.[60] This explanation is also consistent with the small blueshift observed in the laser cavity in Figure 4d, in which photocharging, by slightly bleaching the band edge absorption transition, will reduce the refractive index and lead to the observed blueshift. In addition to the noted spectral shift, the intensity of the two modes varies over time and the absolute intensity of the laser cavity emission also increased by a factor of two over 30 minutes. Again, this may be attributable to the same photocharging of the sample;[69–72] partial charging can lower the lasing threshold[69] and thereby produce a brighter laser over exposure time. These experiments suggests that higher stability of the emissive mode may be achieved with light soaking experiments[60] or by use of the QSs as flowed dyes.[31] As importantly, they also show that laser emission under two-photon excitation can be stable without a decrease in intensity over at least 3.6×10^5 laser shorts. The combination of large two-photon cross sections, long gain lifetimes, wide gain bandwidth, and low thresholds for amplified spontaneous emission indicates that QSs may also be strong candidates for nanoparticle-based dye lasers.

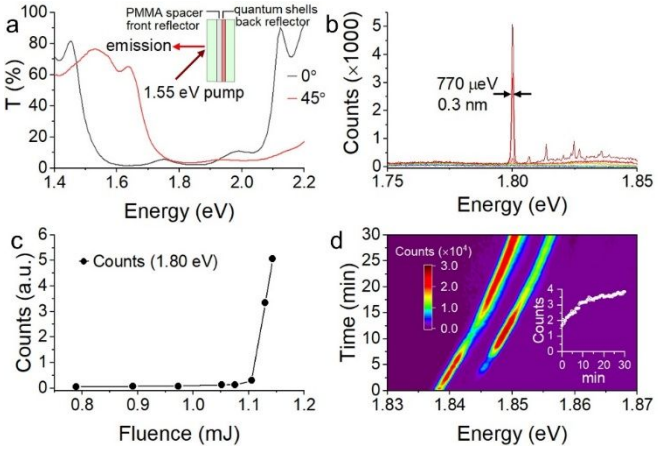

Figure 4. (a) Front window transmission of laser cavity for two-photon pumping of QS sample. The pump beam is directed on to the sample at a 45° angle of incidence and the emission from the cavity is monitored normal to the surface, as shown inset. (b) Photoemission from laser cavity with 8.2 nm core QSs showing and (c) counts at 1.80 eV from the same cavity versus 1.55 eV pump fluence. Violet spectra represent lower fluence and red higher fluence. (d) Spectra as a function of time lapse for a different spot of the same cavity of 8.2 nm core QSs measured at a fixed fluence of 1.3 $mJ \cdot cm^{-2}$ 1.55 eV pump photons.

Conclusions

CdS/CdSe/CdS QSs are shown to have large two-photon cross sections (0.4-7.9×10^6 GM), which make QSs promising nanostructures for upconversion imaging applications. These large two-photon cross-sections are combined with previously-identified advantages of QSs for multiexciton applications.

Under two-photon excitation, QSs show large gain bandwidth (300 meV), long gain lifetime (>5 ns), and slow Auger recombination (>10 ns). Biexciton recombination times reaching greater than 10 ns drives many of these properties. The combination of large non-linear absorption cross-sections with long multiexciton lifetimes results in multimodal, low-threshold, amplified spontaneous emission and lasing under two-photon excitation with thresholds using 1.55 eV pumping as low as 1 $mJ \cdot cm^{-2}$. These QS materials represent some of the most promising materials for the realization of nanocrystal-based dye lasers.

Conflicts of interest

There are no conflicts to declare.

Acknowledgements

Work performed at the Center for Nanoscale Materials, a U.S. Department of Energy Office of Science User Facility, was supported by the U.S. DOE, Office of Basic Energy Sciences, under Contract No. DE-AC02-06CH11357. Work of BGSU team was supported by the award DE-SC0016872. MZ also acknowledges the support by NSF award No. 2208834.

References

1 N. Razgoniaeva, P. Moroz, M. Yang, D. S. Budkina, H. Eckard, M. Augspurger, D. Khon, A. N. Tarnovsky and M. Zamkov, *J. Am. Chem. Soc.*, 2017, **139**, 7815–7822.

2 D. Porotnikov, B. T. Diroll, D. Harankahage, L. Obloy, M. Yang, J. Cassidy, C. Ellison, E. Miller, S. Rogers, A. N. Tarnovsky, R. D. Schaller and M. Zamkov, *Nanoscale*, 2020, **12**, 17426–17436.

3 J. Cassidy and M. Zamkov, *J. Chem. Phys.*, , DOI:10.1063/1.5126423.

4 B. G. Jeong, Y. Park, J. H. Chang, I. Cho, J. K. Kim, K. Char, J. Cho, V. I. Klimov, P. Park, D. C. Lee and W. K. Bae, , DOI:10.1021/acsnano.6b03704.

5 E. A. Dias, J. I. Saari, P. Tyagi and P. Kambhampati, *J. Phys. Chem. C*, 2012, **116**, 5407–5413.

6 N. Wang, S. Koh, B. G. Jeong, D. Lee, W. D. Kim, K. Park, M. K. Nam, K. Lee, Y. Kim, B. H. Lee, K. Lee, W. K. Bae and D. C. Lee, *Nanotechnology*, , DOI:10.1088/1361-6528/aa6828.

7 Z. Meng, B. Mahler, J. Houel, F. Kulzer, G. Ledoux, A. Vasil'ev and C. Dujardin, *Nanoscale*, 2021, **13**, 19578–19586.

8 J. Cassidy, D. Harankahage, D. Porotnikov, A. V. Malko and M. Zamkov, *ACS Energy Lett.*, 2022, **7**, 1202–1213.

9 G. Nagamine, B. G. Jeong, T. A. C. Ferreira, J. H. Chang, K. Park, D. C. Lee, W. K. Bae and L. A. Padilha, *ACS Photonics*, 2020, **7**, 2252–2264.

10 D. Battaglia, J. J. Li, Y. Wang and X. Peng, *Angew. Chem. Int. Ed. Engl.*, 2003, **42**, 5035–9.

11 E. P. Pokatilov, V. A. Fonoberov, V. M. Fomin and J. T. Devreese, *Phys. Rev. B*, 2001, **64**, 245329.

12 M. Braun, S. Link, C. Burda and M. El-Sayed, *Chem. Phys. Lett.*, 2002, **361**, 446–452.

13 A. Hässelbarth, A. Eychmüller, R. Eichberger, M. Giersig, A. Mews and H. Weller, *J. Phys. Chem.*, 1993, **97**, 5333–5340.

14 D. Schooss, A. Mews, A. Eychmüller and H. Weller, *Phys. Rev. B*, 1994, **49**, 17072–17078.

15 J. Xu, M. Xiao, D. Battaglia and X. Peng, *Appl. Phys. Lett.*, 2005, **87**, 1–4.

16 A. Eychmüller, A. Mews and H. Weller, *Chem. Phys. Lett.*, 1993, **208**, 59–62.

17 D. Battaglia, B. Blackman and X. Peng, *J. Am. Chem. Soc.*, 2005, **127**, 10889–97.

18 S. A. Ivanov, A. Piryatinski, J. Nanda, S. Tretiak, K. R. Zavadil, W. O. Wallace, D. Werder and V. I. Klimov, *J. Am. Chem. Soc.*, 2007, **129**, 11708–11719.

19 D. Oron, M. Kazes and U. Banin, *Phys. Rev. B*, 2007, **75**, 035330.

20 J. Cassidy, B. T. Diroll, N. Mondal, D. B. Berkinsky, K. Zhao, D. Harankahage, D. Porotnikov, R. Gately, D. Khon, A. Proppe, M. G. Bawendi, R. D. Schaller, A. V. Malko and M. Zamkov, *ACS Nano*, 2022, **16**, 3017–3026.

21 F. Helmchen and W. Denk, *Nat. Methods*, 2005, **2**, 932–940.

22 W. Denk, J. H. Strickler and W. W. Webb, *Science (80-.).*, 1990, **248**, 73–76.

23 G. S. He, L. S. Tan, Q. Zheng and P. N. Prasad, *Chem. Rev.*, 2008, **108**, 1245–1330.

24 C. Zhang, F. Zhang, T. Zhu, A. Cheng, J. Xu, Q. Zhang, S. E. Mohney, R. H. Henderson and Y. A. Wang, *Opt. Lett.*, 2008, **33**, 2437.

25 J. J. Jasieniak, I. Fortunati, S. Gardin, R. Signorini, R. Bozio, A. Martucci and P. Mulvaney, *Adv. Mater.*, 2008, **20**, 69–73.

26 C. Bauer, B. Schnabel, E.-B. Kley, U. Scherf, H. Giessen and R. F. Mahrt, *Adv. Mater.*, 2002, **14**, 673–676.

27 Y. Wang, V. D. Ta, Y. Gao, T. C. He, R. Chen, E. Mutlugun, H. V. Demir and H. D. Sun, *Adv. Mater.*, 2014, **26**, 2954–2961.

28 G. Xing, Y. Liao, X. Wu, S. Chakrabortty, X. Liu, E. K. L. Yeow, Y. Chan and T. C. Sum, *ACS Nano*, 2012, **6**, 10835–10844.

29 B. Guzelturk, Y. Kelestemur, K. Gungor, A. Yeltik, M. Z. Akgul, Y. Wang, R. Chen, C. Dang, H. Sun and H. V. Demir, *Adv. Mater.*, 2015, **27**, 2741–2746.

30 M. Olutas, B. Guzelturk, Y. Kelestemur, A. Yeltik, S. Delikanli and H. V. Demir, *ACS Nano*, 2015, **9**, 5041–5050.

31 M. Li, M. Zhi, H. Zhu, W.-Y. Y. Wu, Q.-H. H. Xu, M. H. Jhon and Y. Chan, *Nat. Commun.*, 2015, **6**, 1–8.

32 G. S. He, P. P. Markowicz, T.-C. Lin and P. N. Prasad, *Nature*, 2002, **415**, 767–770.

33 Q. Zheng, H. Zhu, S. C. Chen, C. Tang, E. Ma and X. Chen, *Nat. Photonics*, 2013, **7**, 234–239.

34 C. Zhang, C. L. Zou, Y. Yan, R. Hao, F. W. Sun, Z. F. Han, Y. S. Zhao and J. Yao, *J. Am. Chem. Soc.*, 2011, **133**, 7276–7279.

35 C. F. Zhang, Z. W. Dong, G. J. You, S. X. Qian and H. Deng, *Opt. Lett.*, 2006, **31**, 3345.

36 B. T. Diroll, N. Gogotsi and C. B. Murray, *Chem. Mater.*, 2016, **28**, 3345–3351.

37 B. G. Jeong, Y.-S. Park, J. H. Chang, I. Cho, J. K. Kim, H. Kim,

K. Char, J. Cho, V. I. Klimov, P. Park, D. C. Lee and W. K. Bae, *ACS Nano*, 2016, **10**, 9297–9305.
38 A. Sitt, F. Della Sala, G. Menagen and U. Banin, *Nano Lett.*, 2009, **9**, 3470–3476.
39 A. F. Cihan, Y. Kelestemur, B. Guzelturk and H. V. Demir, 2013, **1**, 5–6.
40 F. Garcia-Santamaria, Y. Chen, J. Vela, R. D. Schaller, J. A. Hollingsworth and V. I. Klimov, *Nano Lett.*, 2009, **9**, 3482–3488.
41 V. I. Klimov, *Science*, 2000, **287**, 1011–1013.
42 I. Robel, R. Gresback, U. Kortshagen, R. D. Schaller and V. I. Klimov, *Phys. Rev. Lett.*, 2009, **102**, 177404.
43 C. Melnychuk and P. Guyot-Sionnest, *Chem. Rev.*, 2021, **121**, 2325–2372.
44 Y. S. Park, W. K. Bae, L. A. Padilha, J. M. Pietryga and V. I. Klimov, *Nano Lett.*, 2014, **14**, 396–402.
45 Y. He, S. Hu, T. Han, X. Chen, Y. Yu, T. Li, W. Zhu and G. Ouyang, *ACS Omega*, 2019, **4**, 9198–9203.
46 C. She, I. Fedin, D. S. Dolzhnikov, P. D. Dahlberg, G. S. Engel, R. D. Schaller and D. V. Talapin, *ACS Nano*, 2015, **9**, 9475–9485.
47 V. I. Klimov, *Annu. Rev. Condens. Matter Phys.*, 2014, **5**, 285–316.
48 G. E. Cragg and A. L. Efros, *Nano Lett.*, 2010, **10**, 313–317.
49 R. Scott, A. W. Achtstein, A. Prudnikau, A. Antanovich, S. Christodoulou, I. Moreels, M. Artemyev and U. Woggon, *Nano Lett.*, 2015, **15**, 4985–4992.
50 A. W. Achtstein, A. Ballester, J. L. Movilla, J. Hennig, J. I. Climente, A. Prudnikau, A. Antanovich, R. Scott, M. V. Artemyev, J. Planelles and U. Woggon, *J. Phys. Chem. C*, 2015, **119**, 1260–1267.
51 M. A. Albota, C. Xu and W. W. Webb, *Appl. Opt.*, 1998, **37**, 7352.
52 J. P. Hermann and J. Ducuing, *Opt. Commun.*, 1972, **6**, 101–105.
53 C. Xu and W. W. Webb, *J. Opt. Soc. Am. B*, 1996, **13**, 481.
54 M. Allione, A. Ballester, H. Li, A. Comin, J. L. Movilla, J. I. Climente, L. Manna and I. Moreels, *ACS Nano*, 2013, **7**, 2443–2452.
55 A. Antanovich, A. W. Achtstein, A. Matsukovich, A. Prudnikau, P. Bhaskar, V. Gurin, M. Molinari and M. Artemyev, *Nanoscale*, 2017, **9**, 18042–18053.
56 B. T. Diroll, *Chem. Mater.*, 2020, **32**, 5916–5923.
57 P. Geiregat, R. Tomar, K. Chen, S. Singh, J. M. Hodgkiss and Z. Hens, *J. Phys. Chem. Lett.*, 2019, **10**, 3637–3644.
58 B. T. Diroll, A. Brumberg and R. D. Schaller, *Sci. Rep.*, 2022, **12**, 1–10.
59 G. Nagamine, T. A. C. Ferreira, D. B. Almeida, J. C. Lemus, J. H. Chang, B. G. Jeong, W. K. Bae and L. A. Padilha, *ACS Photonics*, 2021, acsphotonics.1c01293.
60 S. J. Neuhaus, E. Marino, C. B. Murray and C. R. Kagan, *Nano Lett.*, 2023, **23**, 645–651.
61 B. Guzelturk, Y. Kelestemur, M. Z. Akgul, V. K. Sharma and H. V. Demir, *J. Phys. Chem. Lett.*, 2014, **5**, 2214–2218.
62 B. Guzelturk, Y. Kelestemur, M. Olutas, S. Delikanli and H. V. Demir, *ACS Nano*, 2014, **8**, 6599–6605.
63 D. Dede, N. Taghipour, U. Quliyeva, M. Sak, Y. Kelestemur, K. Gungor and H. V. Demir, *Chem. Mater.*, 2019, **31**, 1818–1826.
64 L. Xu, Y. Meng, C. Xu and P. Chen, *RSC Adv.*, 2018, **8**, 36910–36914.
65 Y. Xu, Q. Chen, C. Zhang, R. Wang, H. Wu, X. Zhang, G. Xing, W. W. Yu, X. Wang, Y. Zhang and M. Xiao, *J. Am. Chem. Soc.*, 2016, **138**, 3761–3768.
66 Z. Liu, Z. Hu, Z. Zhang, J. Du, J. Yang, X. Tang, W. Liu and Y. Leng, *ACS Photonics*, 2019, **6**, 3150–3158.
67 J. Ban, Y. Yu, P. Yue, L. Lian, C. Xu, L. Guo and S.-D. Liu, *J. Phys. Chem. C*, 2022, **126**, 8400–8407.
68 J. Xu and M. Xiao, *Appl. Phys. Lett.*, 2005, **87**, 173117.
69 C. Wang, B. L. Wehrenberg, C. Y. Woo and P. Guyot-Sionnest, *J. Phys. Chem. B*, 2004, **108**, 9027–9031.
70 K. Wu, Y. Park, J. Lim and V. I. Klimov, *Nat. Nanotechnol.*, 2017, **12**, 1140–1147.
71 Y. S. Park, J. Roh, B. T. Diroll, R. D. Schaller and V. I. Klimov, *Nat. Rev. Mater.*, 2021, **6**, 382–401.
72 O. V Kozlov, Y. Park, J. Roh, I. Fedin, T. Nakotte and V. I. Klimov, *Science (80-.).*, 2019, **365**, 672–675.